

Characterizing a scatterfield optical platform for semiconductor metrology

B M Barnes¹, R Attota¹, R Quintanilha², Y-J Sohn² and R M Silver¹

¹ National Institute of Standards and Technology, Gaithersburg, MD 20899-8212, USA

² KT Consulting, Antioch, CA 94509, USA

Received 18 June 2010, in final form 5 November 2010

Published 21 December 2010

Online at stacks.iop.org/MST/22/024003

Abstract

Scatterfield microscopy is the union of a high-magnification imaging platform and the angular and/or wavelength control of scatterometry at the sample surface. Scatterfield microscopy uses Köhler illumination, where each point on the source translates to a particular angle of illumination yet also yields spatial illumination homogeneity. To apply scatterfield microscopy to quantitative metrology, several aspects of the optical column must be well understood. Characterizations are presented of the illumination intensity, angle, polarization, and measured glare as functions of the position of an aperture in the conjugate to the back focal plane (CBFP) of the objective lens. The characterization of a reference sample is shown to be as important as the inspection of other optical elements in the optical column. Reflectivity can be derived for line arrays lacking diffractive orders by measuring such a reference and deriving a 'tool function' to account for the current state of the optical platform. Examples from defect, critical dimension, and overlay metrologies are presented to demonstrate the necessity of characterization for scatterfield microscopy.

Keywords: scatterfield microscopy, Köhler illumination, microscope characterization, semiconductor metrology

(Some figures in this article are in colour only in the electronic version)

1. Introduction

The continued use of optical inspection tools with high magnification would be highly advantageous given the relative speed of optical measurements relative to manufacturing processes. However, the smallest line widths, or critical dimensions (CD), of patterned semiconductor devices are not resolved using bright-field optical microscopy. Both patterned defect detection and overlay offset metrology are two continuing applications of this microscopy that face greater challenges as critical dimensions decrease. While scanning probe technologies such as scanning electron microscopy and atomic force microscopy can be used to perform such measurements for device manufacture, these scanning techniques are inherently slow given their serial operation. Optical inspection is inherently parallel, non-destructive, and scalable to meet throughput requirements.

Particularly in CD metrology, measurement steps have been shifting from imaging optical microscopy to scatterometry [1, 2]. In scatterometry, light is aimed onto

a small portion (currently, a spot 30 μm in diameter or less) [3] of a specially designed target, and its reflectivity is captured as a function of incident angles and/or wavelength. Critical dimensions can be obtained from the resultant reflectivity curves by matching against electromagnetic simulations that are based upon a parametric description of the target [4]. For example, a line grating can be defined by the line width, line height, and grating pitch. These three parameters would form the basis for such simulations, performed either in real time as part of a fitting routine or off-line to form a 3D parametric library of curves. In either case, regression is then used to compare measured reflectivity curves to simulated curves to deduce the best set of parameters that describes the given target. The error in such a parameterization is computed taking the derivatives of the reflectivities as functions of the separate parameters, which will reveal cross-correlations among parameters [5].

While research is ongoing to determine methods for comprehending the signals of scatterometry that are produced from targets smaller than the incident spot size [6], an

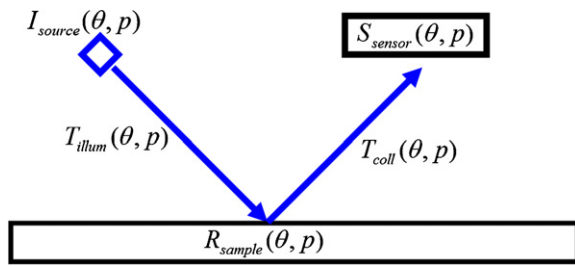


Figure 1. Schematic of a reflective optical platform. The source intensity, I_{source} , differs from the intensity reported by the sensor, I_{meas} , due to effects from the transmissivity of the illumination (T_{illum}) and collection (T_{coll}) paths as well as the inherent reflectivity of the sample studied (R_{sample}) and the sensitivity of the sensor, S_{sensor} . The characterization steps for a scatterfield microscope are designed to determine the effects of T_{illum} and T_{coll} on I_{meas} as functions of polarization, p , and incident angle, θ .

alternative exists for extending the concepts of scatterometry to smaller features, scatterfield microscopy. Scatterfield microscopy is the union of a high-magnification imaging platform and the angular and/or wavelength control of scatterometry at the sample surface [7]. By this definition, scatterfield microscopy may be performed with the imaging sensor at the imaging plane (as is presented here) or at a Fourier plane [8], though the latter has been termed as Fourier scatterometry previously [9]. As in scatterometry, the analysis of the data collected is more ‘signature-based’ than it is ‘image-based.’ For scatterometry and scatterfield microscopy, quantitative CD metrology can be facilitated by the successful matching against electromagnetic simulations.

To illustrate the differences and similarities between scatterometry and scatterfield microscopy, figure 1 shows the schematic layout of an optical system in which the sensor collects the specular reflection of the sample. Variables presented in figure 1 are used in equation (1) to demonstrate the composition of the intensity reported by a sensor, I_{meas} , which is less than the source intensity, I_{source} , due to various modifiers, as

$$I_{meas}(\theta, p) = I_{source}(\theta, p) \times T_{illum}(\theta, p) \times R_{sample}(\theta, p) \times T_{coll}(\theta, p) \times S_{sensor}(\theta, p), \quad (1)$$

where T_{illum} is the transmissivity of the illumination optics between the source and sample, R_{sample} is the reflectivity of the sample, T_{coll} is the transmissivity of the collection path between sample and sensor, and S_{sensor} is the sensitivity of the sensor. All terms are stated as functions of the polarization, p , and the angle of incidence, θ . In the general discussion, θ represents an arbitrary angle of incidence; in some specific examples, the azimuthal angle, ϕ , and the polar angle, θ , will be specified explicitly. Focusing lenses and collection optics are employed in many scatterometers. However, instead of moving the sample or optical column to generate an incident angle as in scatterometry, scatterfield microscopy yields varying angles of incidence though engineering of the illumination; the sample and optics do not move. Thus, the need for characterizing the optical tool increases as high-magnification imaging optics are placed in the illumination and collection paths.

Due to the specific methods by which the illumination is controlled in the National Institute of Standards and Technology (NIST) Visible-light Scatterfield Microscope, the characterization of this component, T_{illum} , is a primary focus of this paper. This analysis is explained and points of consideration for utilizing scatterfield microscopy techniques are presented, including a method for removing the effects of T_{illum} altogether in limited cases. Practical examples for critical dimension metrology, overlay metrology, and defect metrology demonstrate the use of this characterization and the necessity of carrying out scatterometry-type measurements in a high-magnification platform despite the apparent burden of these additional considerations.

2. Characterizations with examples

In this section, the various characterizations are presented with examples taken from the NIST Visible-light Scatterfield Microscope. A previous publication [10] outlines procedures to verify that a scatterfield microscope is in the necessary alignment, thus a more in-depth discussion of the characterization steps required for improved metrology is presented here.

Before discussing the range of tests performed on the optical tool, it is important to specify how the illumination optical column is designed in order to make use of the scattered field. A highly successful method for controlling the angle of incidence at the sample plane in an optical microscope is a well-established method called Köhler illumination [11]. In Köhler illumination, depicted schematically in figure 2(a), the source may be thought of as an ensemble of point sources. Each point source is imaged onto the back focal plane of the condenser lens, which in the present case is the objective lens. One consequence of this imaging is that all points of the source illuminate the sample plane with spatial homogeneity. Rays from the smallest portion of the source illuminate the entire illuminated part of the sample plane evenly across the illuminated spot. If only one part of the source is allowed to pass through the optical column, the sample will still be homogeneously illuminated spatially, but only at one angle of incidence. As the back focal plane of the objective lens is typically very small and difficult or impossible to access, a conjugate to this back focal plane (CBFP) is relayed out and magnified for easier control of the illumination angle. The optical layout for the illumination path of the NIST Visible-light Scatterfield Microscope is shown in figure 2(b). Instead of blocking the source directly, blocking light at this CBFP leads to specific angles of incidence at the sample.

2.1. CBFP position versus incident angle

The mapping of the CBFP position to angle is the most common characterization step performed, as it is required after any changes in the position of mounted optical elements. The relationship between CBFP position and angle of incidence therefore must be understood thoroughly. A computer-controlled x - y stage moves an aperture to allow selected rays of light to pass through the system. One disadvantage to using

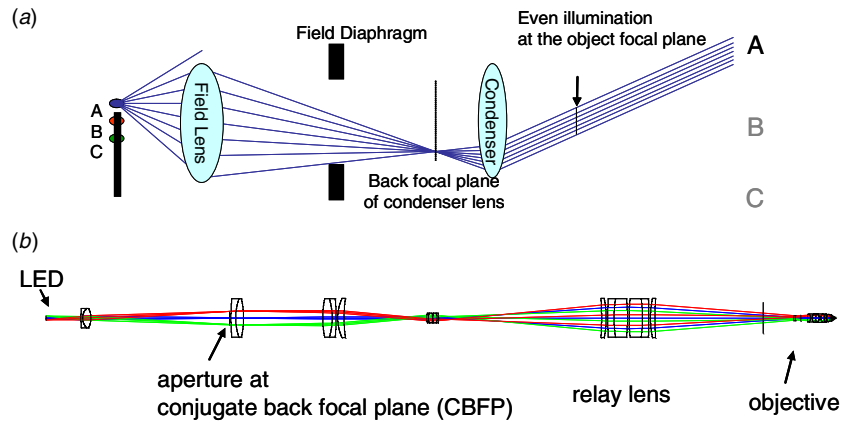


Figure 2. Schematic and ray-trace drawing of a Köhler illumination scheme for scatterfield microscopy. (a) This schematic shows the capability to control incident angle at the sample by blocking parts of the source. (b) The ray trace diagram illustrates the optics required to extract a magnified conjugate to the back focal plane (CBFP) of the objective lens.

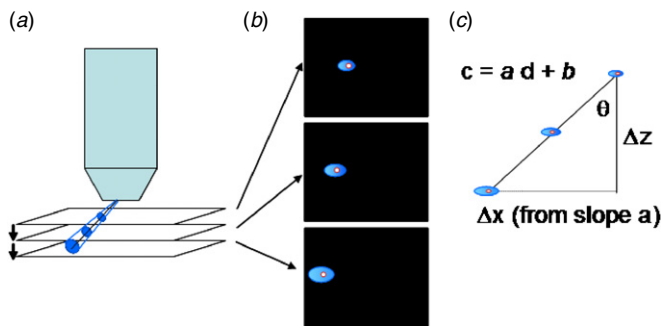


Figure 3. Method for determining the generalized angle of incidence, θ , using a single aperture in the CBFP. (a) A camera measures the conical cross-section of illumination at several distances Δz from the objective. (b) Software is used to extract the weighted center of the intensity in these ellipses. (c) After fitting a line to the positions, the slope, a , of that line and Δz are sufficient for determining θ .

such an aperture is that the majority of the light from the source is wasted. A balance has to be struck between having an aperture small enough to define a narrow cone of angles arriving at the surface and having an aperture large enough to ensure a sufficient amount of reflected light at the sensor. The inherent nature of finite apertures introduces an error into this calibration.

Another attribute of Köhler illumination permits the following method for determining the relationship between CBFP position and angle. In the far field of the objective lens, the image of the source (and thus the image of the aperture in the CBFP) is imaged at infinity. As a very high magnification ($150\times$) objective lens is used in the microscope, small distances (1 mm) from the sample plane are sufficient for the CBFP and any apertures in that plane to be imaged. As shown in figure 3(a), a single aperture rastered in the CBFP yields a dot in this far field that can be measured at different distances from the objective lens. In figure 3(b), this dot appears to cross the field-of-view of the camera as the distance Δz is increased. The camera used is not large enough to capture the highest angles permitted by the numerical aperture, NA, of the objective lens (here,

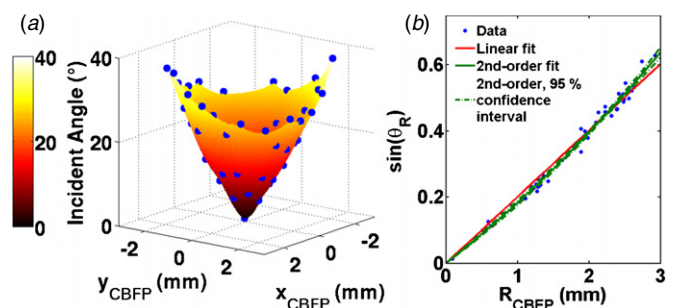


Figure 4. Angle of incidence as a function of the CBFP position. (a) The plot of angles θ relative to the CBFP x - y plane forms a cone that points to CBFP coordinates (x_0, y_0) for which the incidence is normal to the sample. (b) The x - y plane can be reduced to radial coordinates once (x_0, y_0) is determined. Radial position in the CBFP is plotted against $\sin(\theta)$. This nominally linear relationship is shown with linear and second-order polynomial fits.

$NA = 0.95$, or 72°) and the planar surface of the camera ensures that off-axis illumination forms an elliptical conical cross-section on the camera. Commercial software is used to identify the single dot on each image and to determine its center-of-mass in a Cartesian pixel space. Foreknowledge of the pixel spacing in micrometers allows determination of the changes in point location, while Δz is determined from the computer control of the coarse-focus motors. As shown in figure 3(c), knowledge of the slope connecting these centers-of-mass and Δz provides a relative determination Δx (and Δy) relative to the optical axis, leading to an angle of incidence for each CBFP position. The angle of incidence is shown as a function of (x_{CBFP}, y_{CBFP}) in figure 4(a).

Nominally, the lines joining the centers-of-mass should point toward the optical axis, and there should be a single CBFP position on this axis that yields a normal incidence beam. After determining this (x_0, y_0) position in the CBFP, each position can then be calculated as a radial distance R_{CBFP} . A plot of the sine of the incident angle as a function of R_{CBFP} is shown in figure 4(b) along with linear and second-order polynomial fits, each assuming a zero intercept. A linear relationship between $\sin(\theta)$ and R_{CBFP} should be expected,

but these data deviated slightly from this ideal. A 95% confidence interval is shown for the second-order polynomial fit to estimate the uncertainty in angle. Here, all contributing components of the uncertainty are determined solely from the statistical analysis of these observations. As some points fall outside these confidence bands, the fitting model chosen is not rigorous. If these bands are assumed valid, uncertainties in the angle can be calculated for a 95% level of confidence. For a 10° angle, this uncertainty would be $\pm 0.11^\circ$ while for a 30° angle the uncertainty would be $\pm 0.28^\circ$. Radial symmetry is assumed for figure 4(b), and a clear absence of symmetry is a signal to realign. A poorer choice of (x_0, y_0) would lead to a broader distribution of points about the fit, though even the best choice of (x_0, y_0) still yields some random distribution about this fit due to the finite cone of angles and the pixelation of the camera.

It is advantageous to use the aperture to be used in scatterfield data collection as the aperture for this calibration in order to establish this (x_0, y_0) normal incidence position in the CBFP. An alternative approach [12] has been developed for use on the NIST 193 nm Scatterfield Microscope, which features a catadioptric objective that inherently blocks normally incident light. An array of apertures of known separation is placed in the CBFP and imaged with a camera placed at several values of Δz . Data are acquired much quicker than through serial rastering but additional steps are required to relate a subsequent single aperture to the optical axis.

2.2. Incident angle versus intensity

Köhler illumination is designed to illuminate the sample plane homogeneously. That is, every point on the source evenly fills the illuminated spot on the sample. Permitting only part of the source to illuminate the sample limits the angles of illumination yet the spatial homogeneity is preserved. As with any extended source its intensity inhomogeneity becomes apparent when examining the relationship between incident angle and intensity. Angular intensity homogeneity is not guaranteed from Köhler illumination, and angular inhomogeneity can have a profound effect upon scatterfield microscopy measurements [10].

Characterization of the intensity can be performed using a variety of methods. The most thorough examination of the illumination intensity has an aperture moving in the CBFP while the light is collected from the objective using a photodiode mounted onto an integrating sphere. The integrating sphere collects light at higher angles than possible with the under-objective camera used for the angle characterization above. The light entering the sphere is reflected within the sphere several times, finally being collected by this photodiode. Its baffling is imperfect, thus the sphere was rotated about the optical axis to three angular positions to isolate the measured asymmetry due to the baffle. This asymmetry has been subtracted from the data shown in figure 5. The intensity decreases as a function of increasing R_{CBFP} position, and hence also as a function of increasing incident angle.

Such maps can be applied to interpret the optical response from the sample by scaling the results of electromagnetic

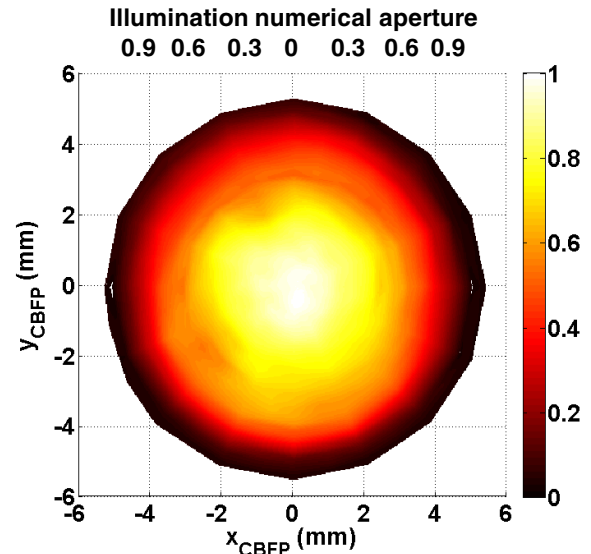


Figure 5. Illumination intensity as a function of the CBFP x - y plane position for unpolarized light. The plane has been centered using the nominal optical axis. Measurements were made by capturing the light from the objective with an integrating sphere underneath, and a photodiode on one port of that sphere. Data are corrected to subtract asymmetries caused by the baffle. A slight shift in the source position after a calibration renders the illumination numerical aperture values shown approximate, emphasizing the continual need for illumination calibration.

simulations to the output of the microscope. However, in practice it is the signal from the microscope that is scaled to be comparable to the output of the electromagnetic simulations and analytical solutions, for example the Fresnel equations for reflectivity from a planar surface. To perform such comparisons, the sample reflectivity from equation (1), R_{sample} , must be extracted from the multiple terms that comprise I_{meas} . A simple way to determine R_{sample} is to measure a second sample with a well-known reflectivity using the same optical configuration and experimental conditions. The resulting intensity measurements can be divided to yield

$$\frac{I_{\text{meas},1}}{I_{\text{meas},2}} = \frac{R_{\text{sample},1}(\theta_{\text{inc}}, p) T_{\text{coll}}(\theta_1, p) \times S_{\text{sensor}}(\theta_1, p)}{R_{\text{sample},2}(\theta_{\text{inc}}, p) T_{\text{coll}}(\theta_2, p) \times S_{\text{sensor}}(\theta_2, p)}, \quad (2)$$

where θ_{inc} is the angle of incidence and θ_1 and θ_2 are the angles reflected from each sample. The illumination path transmissivity and the source intensity cancel out immediately. The reflectivities will differ, but the collection path transmissivity and sensor effects will cancel out if $\theta_1 = \theta_2$. Often a characterized mirror or bare silicon surface is used as $R_{\text{sample},2}$ and as a planar reflector, $\theta_2 = -\theta_{\text{inc}}$. $R_{\text{sample},2}$ may either be known analytically given its optical constants n and k , or determined from an experimental calibration.

If the unknown sample is unpatterned or sufficiently dense and periodic, such as a line grating with pitch, p , that is less than the wavelength, λ , then there will be angular range for which collection angle $\theta_1 = -\theta_{\text{inc}}$. For less dense periodic structures ($p > \lambda$) and isolated structures, this simple angular relation does not hold due to higher order diffraction that is

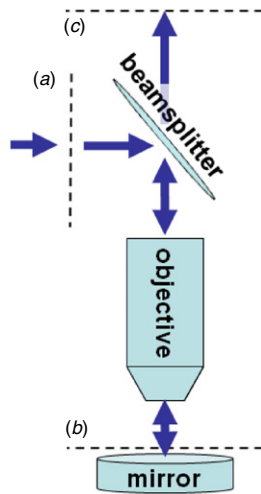


Figure 6. Sensor positions for the determination of polarization effects at the sample and sensor. Light was collected using a photodiode (a) before the beamsplitter, (b) after the beamsplitter, and (c) after reflection through the splitter a second time. The pellicle beamsplitter that was characterized is a polarizing element.

collected at various angles by the objective lens for planar reflectors and dense periodic structures,

$$R_{\text{sample},1}(\theta, p) = \frac{I_{\text{meas},1}(\theta, p) \times R_{\text{sample},2}(\theta, p)}{I_{\text{meas},2}(\theta, p)}. \quad (3)$$

The range of incident angles over which equation (3) remains valid can be demonstrated using the following example. An array of lines with pitch 300 nm illuminated with $\lambda = 450$ nm light produces an $m = 1$ diffraction order when $\theta > 30^\circ$. Furthermore, when $\theta > 33^\circ$, $\theta_{m=1} < 72^\circ$, which means that the order is rocked into an objective lens if it has a collection numerical aperture of 0.95 or larger. These higher orders of diffraction can be removed if $m = \pm 1 \dots \pm n$ orders are physically blocked at a Fourier plane in the collection path to permit only $m = 0$ light to reach the sensor, but such an order-blocking scheme is not yet in place on the NIST Visible-light Scatterfield Microscope.

Therefore, the limitations of the characterization of the microscope place limits on its current capabilities for qualitative and/or quantitative metrology, as will be discussed in section 3.

2.3. Other characterizations

The addition of several optical elements between the source and sensor introduces multiple opportunities for polarization effects and glare to influence the results. These effects are best described through examples from the NIST Visible-light Scatterfield Microscope.

The choice of a pellicle beamsplitter yielded benefits in preparing the optomechanical layout at the cost of polarization effects at the sample and at the sensor. To examine these effects, light was collected by a photodiode (a) in front of the pellicle beamsplitter, (b) after reflection off the beamsplitter, and (c) after the light is reflected from a mirror below and transmitted again through the beamsplitter. Figure 6 is a schematic showing these three locations. The mean ratio of

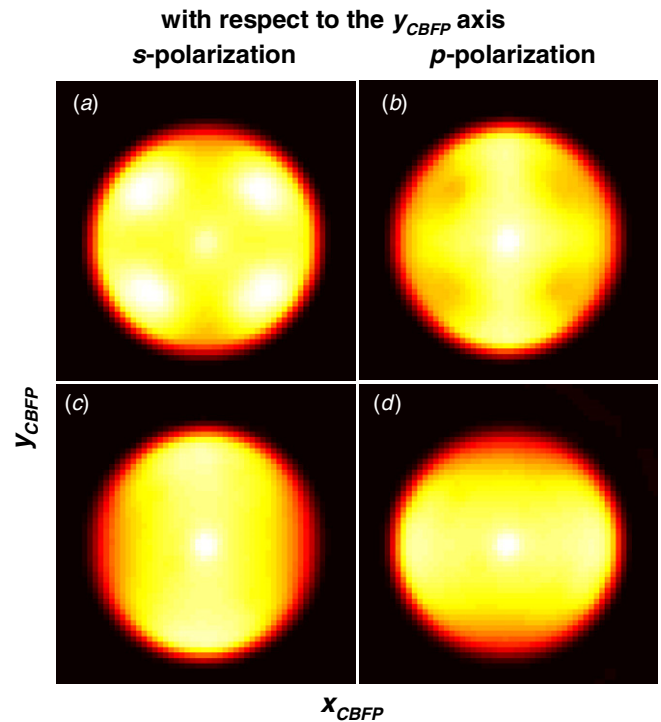


Figure 7. Measured reflected intensity from a dielectric mirror and from blank Si. Polarization is defined with respect to the Y_{CBFP} axis. (a) Dielectric mirror illuminated by s-polarized light, (b) dielectric mirror, p-polarized light, (c) bare silicon, s-polarized light, (d) bare silicon, p-polarized light. Characterization of a reference sample is important for proper normalization for many scatterfield experiments. Graph from [12].

the intensities of p- to s-polarized light upon the beamsplitter was 1, as there was no inherent polarization to the source or the optics. Upon reflection by the beamsplitter, the mean intensity ratio of p- to s-polarized light dropped to 0.63. Some of the polarization effect was reversed as the reflected light returned through the beamsplitter, as the ratio of p- to s-polarized light was 0.75. These values are provided to reiterate that each part of a scatterfield microscope must be characterized and its effects upon the measured intensity must be considered. As equation (3) is a ratio of two measured intensities, it is necessary that both are measured using the same optical setup to negate these type of effects.

However, another element in the optical path that is susceptible to polarization effects is the reference sample itself. Figures 7(a) and (b), first presented in [13], show the measured intensity reflected from a dielectric mirror. While this mirror is a nearly uniform reflector along the azimuthal $\phi = 0^\circ$ and $\phi = 90^\circ$ angular directions, this type of mirror is a poor reference when ϕ is not in one of these orthogonal directions. In figures 7(c) and (d), the reflectivity of silicon is shown to be polarization dependent as expected but there are not dramatic changes at $\phi = 45^\circ$, for example. In scatterfield microscopy, the characterization of a reference sample is as important as any other optical element in the illumination and collection paths.

The small dot in the center of each graph in figure 7 is due to glare within the optical microscope. Glare is measured by

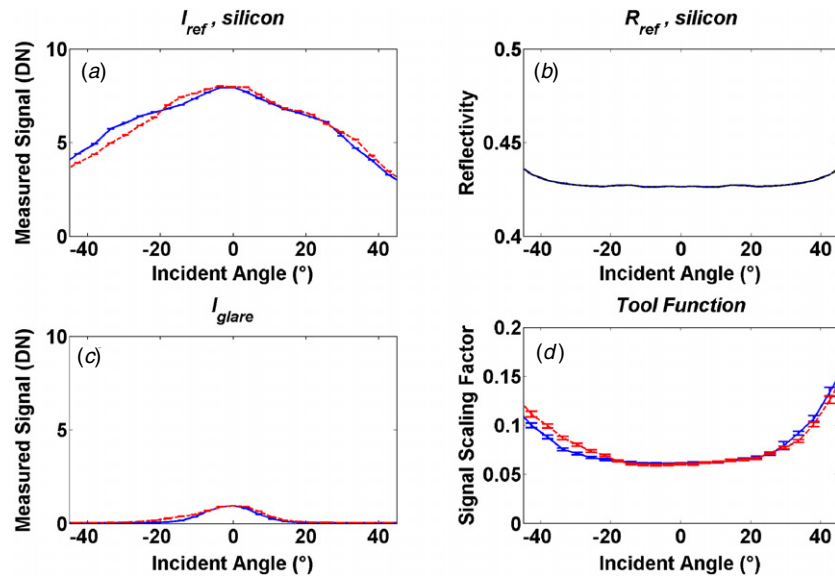


Figure 8. Graphical derivation of the tool function through the use of blank silicon. The solid line is for $\phi = 0^\circ$ and the dotted line, $\phi = 90^\circ$. (a) I_{ref} , measured, expressed in digital number (DN) from the camera. (b) R_{ref} , known from theory. (c) I_{glare} , measured. (d) The tool function, $\text{TF} = R_{\text{ref}}/(I_{\text{ref}} - I_{\text{glare}})$. The reflectivity of an unknown is obtained by multiplying the tool function against I_{meas} . Though this example is for unpolarized light, the tool function must be determined for all polarizations used.

placing the objective within a cup coated internally with black anti-reflective flocking and performing the experiment as if a sample were in focus, with the illumination system activated. Detection in the absence of a target indicates back reflections present within the microscope. It is highly dependent upon angle and to a lesser extent, polarization. While glare can be partially mitigated through improvements to the field stop and through internal flocking, it has not yet been permanently eradicated. Glare must be measured and subtracted from the intensities as described below.

2.4. The tool function

Glare removal is a final step toward deriving a single quantity with which the measured intensity of targets may be converted into reflectivities. Figure 8 shows graphically the composition of the tool function, TF, which can be expressed as

$$\text{TF}(\theta, p) = \frac{R_{\text{ref}}(\theta, p)}{I_{\text{ref}}(\theta, p) - I_{\text{glare}}(\theta, p)}, \quad (4)$$

where the target is assumed to have a zero-order response and the measured intensity of the reference is explicitly corrected by the measurement of the glare. A by-product of correcting for the glare is that there is no need to correct the intensity measurement for the dark current of the charge-coupled device (CCD) camera used to capture the images—the term is common to both I_{ref} and I_{glare} . Equation (3) may be rewritten as

$$R_{\text{target}}(\theta, p) = (I_{\text{meas}}(\theta, p) - I_{\text{glare}}(\theta, p)) \times \text{TF}(\theta, p), \quad (5)$$

which takes glare into account for the target measurement as well.

3. Applications

Three brief examples of the use of scatterfield microscopy are presented below. The examples span from qualitative to quantitative metrology, and an increased rigor in the analysis leads to an increased need for characterization of the optical microscope.

3.1. Defect metrology

Scatterfield inspection of patterned devices for semiconductor patterning defect inspection immediately involves the measurement of reflected light with multiple orders. Therefore, reflectivity is not reported, but intensity only. For this application CBFP position to angle mapping is most important. In defect metrology, die-to-database comparisons are made to detect the presence of a defect. An image of a defect-containing die is compared against an image from a well-patterned die and strong optical response in the difference image reveals the defect. Some defects and die are highly directional, and may not be observable when measured with on-axis illumination. Off-axis illumination for a given set of θ and ϕ may enhance the detection of a defect, as shown in figure 9. Proper characterization of the incident angle is necessary to facilitate this qualitative metrology.

3.2. Overlay metrology

The following example requires characterization of the intensity, angle, polarization, and glare in order to yield valid results. In [15], a successful demonstration of overlay sensitivity using angle-resolved scatterfield microscopy was demonstrated for a grating target consisting of vias in a layer of TEOS over amorphous silicon (aSi) lines, as shown in figure 10. Two targets nominally possessing 0 and 25 nm

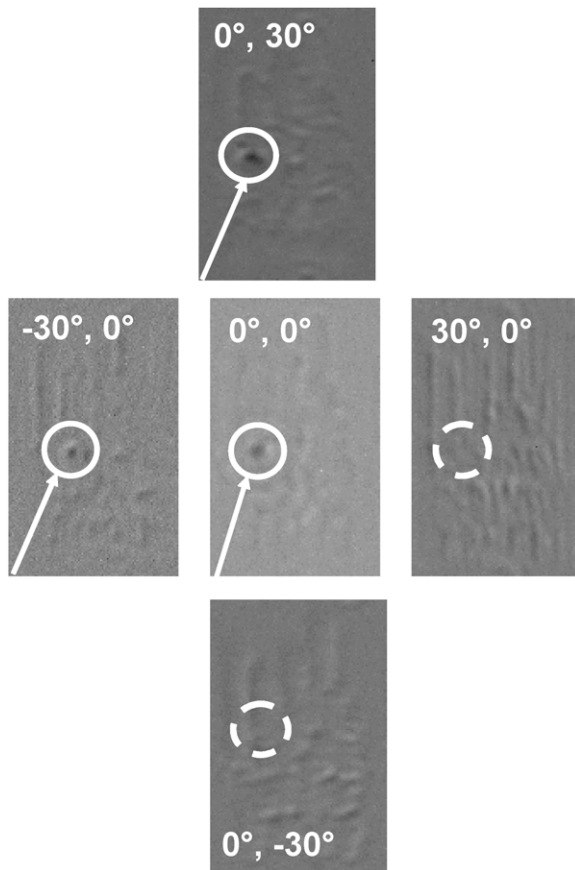


Figure 9. Difference images obtained by subtracting non-defect images from defect images, collected both on- and off-axes. The use of off-axis illumination is important for the detection of certain defects. The defect measured is a line extension in the x direction, which accounts for the directionality of the optical response. Feature size was measured by SEM to be 45 nm, which for these images corresponds to $\lambda/10$. Graph from [14].

overlay were measured, and perpendicular scans across the target, using either linear polarization, showed clear distinctions between the two overlay values. Quantitative overlay measurement would follow from calibration of this sensitivity against targets possessing well-characterized overlay offsets.

The reflectivity values presented in figure 10 were obtained on an older microscope, the NIST Overlay Tool. This tool has been retrofitted with an x - y computer-controlled aperture in its CBFP. Though the diameter of this CBFP is only 2 mm, characterization of this tool has led to its successful use in scatterfield microscopy. A tool function unique to this microscope was applied against the measured intensity from these zero-order overlay targets to obtain the reflectivity curves shown. This overlay result is a clear demonstration of the applicability of scatterfield microscopy concepts to any microscope that has an accessible conjugate to the back focal plane of the objective lens.

3.3. Critical dimension metrology

The accuracy of the characterization of the tool can directly impact the values obtained in quantitative scatterfield

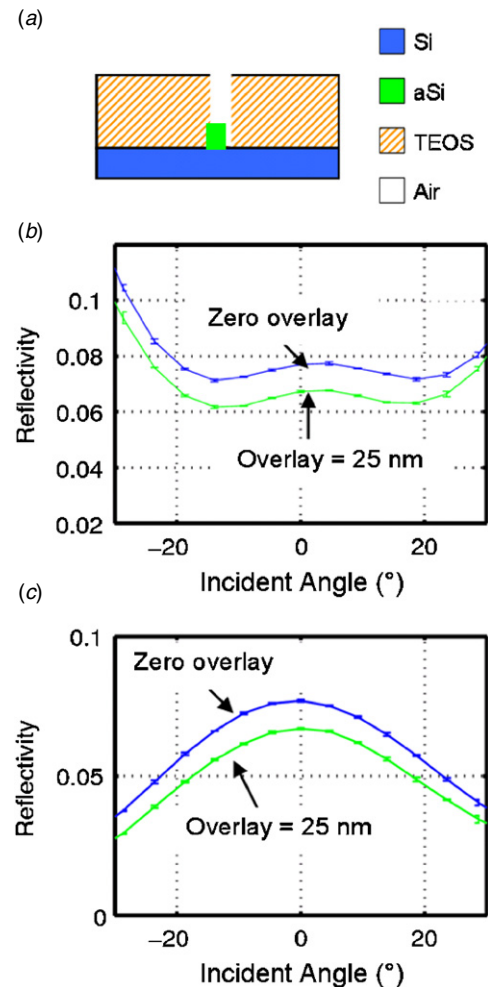


Figure 10. Measured reflectivity curves obtained from scanning perpendicular to an overlay metrology target using polarized, $\lambda = 546$ nm light on the NIST Overlay Tool. (a) Schematic (not to scale) of the grating target, a via in a TEOS layer shown with an overlay offset with respect to aSi lines. (b) p-polarization. (c) s-polarization. While the 25 nm offset is known *a priori* and not from parametric fitting, the sensitivity of scatterfield to changes in overlay is readily apparent. Graph from [15].

microscopy. Scatterometry targets are often gratings that are larger than the spot size of the incident beam. Such targets are often used in scatterfield microscopy, though scatterfield does not require the target to fill the field-of-view. The line width is the critical dimension (CD), while the line height and pitch may also be deduced from parametric fitting of measured reflectivity results against a library of simulated reflectivity curves. These curves are based upon a geometrical description of the cross-section defined by the specific values of CD, height, pitch, etc. With ever-decreasing CD and pitch, such targets present no scattering orders when examined using $\lambda = 450$ nm light as used on the NIST Visible-light Scatterfield Microscope. Thus, reflectivity can be measured by measuring a known reference and applying equation (3) above. In figure 11, four angle scans of a particular target are shown. Reflectivity measurements were performed as a function of incident angle either across or along the grating, and the polarization pass axis was either along or across the

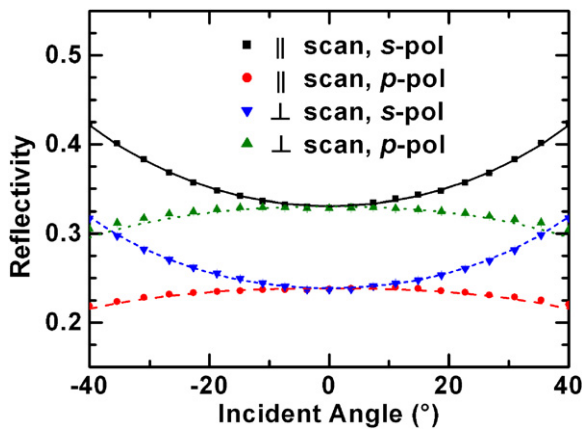


Figure 11. Critical dimension (CD) metrology through parametric fitting of measured reflectivity curves. The polarizations and scan directions for the four curves are shown in the legend. Five parameters were floated for this simulation. The best fit was determined to be: $CD_{\text{line, top}} = 45$ nm, $CD_{\text{line, middle}} = 61$ nm, $CD_{\text{line, bottom}} = 67$ nm, height = 55 nm; the value of the optical constant n was varied but matched its nominal value.

grating, yielding four combinations. The simulated reflectivity curves which best fit the measured data are also plotted. Quantitative critical dimension metrology is achieved through such parametric fitting. Minimal error in the angle mapping and knowledge of the incident intensity as a function of polarization and angle are critical to the performance of these parametric fits.

4. Conclusion

The measurement of various types of targets can be enhanced through the use of scatterfield microscopy. For the results of a scatterfield experiment to have meaning for metrology, multiple types of characterization are required. While the relative ease of scatterometry may make scatterfield microscopy seem cumbersome by comparison, the ever-decreasing size of semiconductor wafer features suggests the preparation of scatterometry-like metrologies that can measure a target or multiple targets within a reduced field-of-view. With this goal, a set of best practices for scatterfield microscopy characterization is being developed and refined.

Acknowledgments

The authors would like to thank Dr Thomas Germer and Dr Steven Brown, both of the NIST Physical Measurement Laboratory, for electromagnetic modeling development and for the loan of an integrating sphere, respectfully. The authors also thank ISMI/SEMATECH³ and the NanoFab of NIST for wafer fabrication and measurement support. They are grateful

for financial support from ISMI, the Office of Microelectronics Programs at NIST and the Scatterfield Optical Competence also from NIST.

References

- [1] Raymond C J, Murnane M R, Sohail S, Naqvi H and McNeil J R 1995 Metrology of subwavelength photoresist gratings using optical scatterometry *J. Vac. Sci. Technol. B* **13** 1484–95
- [2] Minhas B K, Coulombe S A, Naqvi S S H and McNeil J R 1998 Ellipsometric scatterometry for the metrology of sub-0.1- μm -linewidth structures *Appl. Opt.* **37** 5112–5
- [3] Markwort L, Kappel C, Kharrazian R and Guittet P 2010 Full wafer macro-CD imaging for excursion control of fast patterning processes *Proc. SPIE* **7638** 763807
- [4] Logofătu P C 2002 Sensitivity analysis of grating parameter estimation *Appl. Opt.* **41** 7179–86
- [5] Silver R, Germer T, Attota R, Barnes B M, Bunday B, Allgair J, Marx E and Jun J 2007 Fundamental limits of optical critical dimension metrology: a simulation study *Proc. SPIE* **6518** 65180U
- [6] Foldyna M., Licitra C. and De Martino A 2010 Stability of polarimetric grating characterization with beam spot larger than grating box *Proc. SPIE* **7638** 763811
- [7] Silver R M, Barnes B M, Attota R, Jun J, Stocker M, Marx E and Patrick H J 2007 Scatterfield microscopy for extending the limits of image-based optical metrology *Appl. Opt.* **46** 4248–57
- [8] Patrick H J, Attota R, Barnes B M, Germer T A, Dixon R G, Stocker M T, Silver R M and Bishop M R 2008 Optical critical dimension measurement of silicon grating targets using back focal plane scatterfield microscopy *J. Micro/Nanolith. MEMS MOEMS* **7** 013012
- [9] Boher P, Petit J, Leroux T, Foucher J, Desieres Y, Hazart J and Chaton P 2005 Optical Fourier transform scatterometry for LER and LWR metrology *Proc. SPIE* **5752** 192–203
- [10] Barnes B M, Howard L P and Silver R M 2006 Illumination optimization for optical semiconductor metrology *Proc. SPIE* **6289** 62890P
- [11] Köhler A 1883 Ein neues Beleuchtungsverfahren für mikrophotographische Zwecke. *Z. f. Wiss. Mikroskopie* **10** 433
Evannet P J 1994 *Köhler Illumination Centenary: A collection of papers detailing Köhler illumination* (Oxford: Royal Microscopical Society) pp 1–30
- [12] Quintanilha R, Sohn Y J, Barnes B M and Silver R 2010 Sub-50-nm critical dimension measurements using a 193-nm angle-resolved scatterfield microscope *Proc. SPIE* **7638** 76381E
- [13] Barnes B M, Howard L P, Jun J, Lipscomb P and Silver R M 2007 Zero-order imaging of device-sized overlay targets using scatterfield microscopy *Proc. SPIE* **6518** 65180F
- [14] Silver R M, Barnes B M, Sohn Y, Quintanilha R, Zhou H, Deeb C, Johnson M, Goodwin M and Patel D 2010 The limits and extensibility of optical patterned defect inspection *Proc. SPIE* **7638** 76380J
- [15] Attota R, Stocker M, Silver R, Heckert A, Zhou H, Kasica R, Chen L, Dixon R, Orji G, Barnes B and Lipscomb P 2009 Through-focus scanning and scatterfield optical methods for advanced overlay target analysis *Proc. SPIE* **7272** 727214

³ The identification of any commercial product or trade name does not imply endorsement or recommendation by the National Institute of Standards and Technology.